




Article

Investigation of the Solid Solution Hardening Mechanism of Low-Alloyed Copper–Scandium Alloys

Ramona Henle ^{1,*}, Simon Kött ², Norbert Jost ², Gerrit Nandi ¹, Julia Dölling ³, Andreas Zilly ³
and Ulrich Prahl ⁴

- ¹ Faculty of Technology, Cooperative State University Heidenheim, Marienstraße 20, 89518 Heidenheim an der Brenz, Germany; gerrit.nandi@dhbw-heidenheim.de
- ² Institute for Materials and Material Technologies (IWWT), Pforzheim University, Tiefenbronner Straße 65, 75175 Pforzheim, Germany; simon.koett@hs-pforzheim.de (S.K.); norbert.jost@hs-pforzheim.de (N.J.)
- ³ Faculty of Technology, Cooperative State University Stuttgart, Lerchenstraße 1, 70194 Stuttgart, Germany; julia.doelling@dhbw-stuttgart.de (J.D.); andreas.zilly@dhbw-stuttgart.de (A.Z.)
- ⁴ Institute of Metal Forming, Technische Universität Bergakademie Freiberg, Bernhard-von-Cotta Straße 4, 09599 Freiberg, Germany; ulrich.prahl@imf.tu-freiberg.de
- * Correspondence: ramona.henle@dhbw-heidenheim.de

Abstract: The addition of alloying elements is a crucial factor in improving the mechanical properties of pure copper, particularly in terms of enhancing its yield strength and hardness. This study examines the influence of scandium additions (up to 0.27 wt.%) on low-alloyed copper. Following the casting and solution-annealing processes, the alloys were quenched in water to maintain a supersaturated state. The mechanical properties were evaluated by tensile tests to measure the yield strength and the dynamic resonance method to determine the modulus of rigidity. Additionally, X-ray diffraction was utilized to analyze changes in lattice parameters, elucidating the structural modifications induced by scandium. This study dissects the parastic and dielastic effects underlying the solid solution hardening mechanism, providing insights into how scandium alters copper's mechanical properties. The findings align with the solid solution hardening theories proposed by Fleischer and Labusch, providing a comprehensive understanding of the observed phenomena.

Keywords: Cu-Sc alloy; solid solution hardening; atomic size misfit; elastic modulus misfit; yield strength; grain boundary hardening; X-ray diffraction; SEM; tensile test



Citation: Henle, R.; Kött, S.; Jost, N.; Nandi, G.; Dölling, J.; Zilly, A.; Prahl, U. Investigation of the Solid Solution Hardening Mechanism of Low-Alloyed Copper–Scandium Alloys. *Metals* **2024**, *14*, 831. <https://doi.org/10.3390/met14070831>

Academic Editors: Chongze Hu and Xin Wang

Received: 26 June 2024
Revised: 15 July 2024
Accepted: 16 July 2024
Published: 20 July 2024



Copyright: © 2024 by the authors. Licensee MDPI, Basel, Switzerland. This article is an open access article distributed under the terms and conditions of the Creative Commons Attribution (CC BY) license (<https://creativecommons.org/licenses/by/4.0/>).

1. Introduction

Copper alloys play an indispensable role in high-performance applications, such as within the electrical and automotive industries, in which high levels of thermal and electrical conductivity are of crucial importance. Despite these outstanding properties, the comparatively low mechanical strength of pure copper poses a challenge [1]. In order to counteract this deficit, it is common practice to increase the strength of pure copper by alloying it in conjunction with a suitable heat treatment [2–6].

In recent years, copper–scandium alloys (Cu-Sc) have increasingly come into focus as promising candidates for applications with specific requirements for high levels of strength combined with high levels of electrical conductivity. Recent studies by Franczak et al. [7] and Dölling et al. [8] have shown that the combination of copper and scandium has considerable potential in this area and also has advantages in terms of recrystallisation behavior and grain refinement [9]. These investigations primarily focused on the influence of precipitation on its hardness and electrical conductivity, as well as the effect of cold working prior to heat treatment. In a previous study, Henle et al. [10] investigated this effect using differential scanning calorimetry (DSC) measurements on Cu-Sc. The findings indicated that specimens with a 75% cross-section reduction from cold rolling exhibited an earlier onset of the precipitation reaction, which significantly lowered the activation energy.

In comparison to the industrial benchmark alloy Cu-Cr, the application of moderate pre-deformation prior to heat treatment not only resulted in enhanced hardness and electrical conductivity but also initiated the precipitation reaction at lower temperatures [11]. This is advantageous for industrial applications, as it can lead to energy savings and potentially enhance the economic feasibility and performance of these alloys. However, detailed investigations of the strength-enhancing mechanisms and their interactions in such alloys have yet to be documented in the literature.

Despite the low maximum solubility of scandium in the copper matrix of 0.35 wt.% at 865 °C [12–15], as shown in the phase diagram in Appendix B, Figure A1, studies have demonstrated an increase in hardness of up to 30 HV_{0.1} by adding 0.35 wt.% scandium in the solution-annealed state compared to soft-annealed copper [8].

This study is the first step towards a detailed analysis of the strength-enhancing mechanisms of this alloy, focusing on solid solution hardening. To isolate this from other strengthening mechanisms, such as grain boundary hardening, further experimental investigations on grain size are carried out. A comprehensive understanding of the parastic and dielastic interactions of the alloying elements is crucial to accurately describe the mechanism of solid solution hardening in Cu-Sc alloys [16]. The aim of the investigations is to analyze the effects of the interactions in more detail and to predict the critical resolved shear stress or yield strength using the common models of Fleischer et al. [17], Labusch et al. [18], and Gypen et al. [19]. The results are then compared with experimentally determined data. A comprehensive understanding of the mechanisms that increase strength significantly helps to optimize future alloy development.

2. Theoretical Background

An increase in strength is achieved by increasing the plastic deformation resistance, which includes both the movement and the formation of dislocations [20]. In general, the strength can be approximately quantified by the superposition of different hardening mechanisms. This approach is illustrated by the following equation [4]:

$$\sigma_y = \sigma_0 + \sigma_{HP} + \sigma_{dis} + \sigma_{ss} + \sigma_p \quad (1)$$

where σ_y is the yield strength, σ_0 the lattice frictional stress, σ_{HP} is the grain size-dependent strength contribution, σ_{dis} is the hardening due to dislocations, σ_{ss} is the solid solution hardening, and σ_p is the precipitation hardening.

In analogy to the stress intensity factor in linear fracture mechanics, which quantifies the peak stress fields around cracks and describes their effect on crack propagation [21], the Hall–Petch constant is used for the grain size-dependent strength contribution. The relationship between strength and grain size is given by the Hall–Petch equation as follows [22–24]:

$$\sigma_{HP} = \frac{k_{HP}}{\sqrt{d}} \quad (2)$$

where d is the grain size, and k_{HP} is the Hall–Petch constant. The values of this constant vary for different materials and are documented to be 0.11 – 0.14 MPa·√m [2,25–28] for copper.

Solid solution strengthening σ_{ss} is based on the interaction of dislocations with foreign atoms that are incorporated into the lattice substitutionally or interstitially. A distinction is made between parastic, dielastic, and chemical interactions. The chemical interaction results from the change in the stacking fault energy due to the dissolved atoms, which generally decreases with increasing alloy content [2]. A lower stacking fault energy allows for a preferential planar sliding motion of the dislocations in the lattice so that transverse sliding through screw dislocations only occurs at high degrees of deformation and/or temperatures [20]. The most important theories of solid solution strengthening can be illustrated by using different exponents and strengthening parameters.

The parastic effect in the solid solution is caused by atomic size differences between matrix and impurity atoms, which cause compressive or tensile stresses in the crystal

lattice depending on whether the embedded atom is larger or smaller [6,29]. The parelastic interaction δ can be described by the change in the lattice parameters as a function of the alloy content [17].

$$\delta = \frac{1}{a} \cdot \frac{a}{c} \quad (3)$$

where a is the lattice parameter, and c is the alloy content.

In addition, the incorporation of impurity atoms locally changes the bond ratios between the impurity atom and the matrix and thus the stiffness in the solid solution. The elastic energy content of the distortion field of the dislocation is therefore subject to variations. The change in stiffness due to the incorporation of impurity atoms can be described by the change in the shear modulus as a function of the impurity concentration. According to Fleischer et al. [17], the parameter η' is defined as follows:

$$\eta' = \frac{\eta}{1 + 0.5|\eta|} \text{ with } \eta = \frac{1}{G} \cdot \frac{dG}{dc} \quad (4)$$

where G is the shear modulus, and c is the alloy content. It should be noted that screw dislocations have a very low hydrostatic contribution to the stress field and therefore hardly interact with impurity atoms, which have an isotropic distortion field [30,31].

Gypen et al. [19] (henceforth referred to as GD) have proposed a modified modulus parameter η_{GD} based on investigations by Takeuchi et al., which considers the dependence of the shear modulus on the lattice contraction or expansion caused by the dissolved impurity atoms.

$$\eta_{GD} = \frac{\eta + A\delta}{1 + 0.5|\eta + A\delta|} \quad (5)$$

where $A = 5$ for Cu alloys [32]. In the case of $\delta = 0$, this equation changes to the original equation of Fleischer [19].

The modulus effect and the changes in the lattice parameters can now be combined into a hardening parameter according to the theories of Fleischer (henceforth referred to as Fl) and Labusch (henceforth referred to as La) as follows:

$$\varepsilon_{Fl} = |\eta' + \alpha\delta| \quad \varepsilon_{La} = \sqrt{(\eta'^2 + (\alpha\delta)^2)} \quad (6)$$

where α is a weighting parameter that considers the influence of the parelastic and dielastic effects and provides information on which type of dislocation interacts with the impurity atoms. In general, $3 < \alpha < 16$ applies for screw dislocations and $\alpha > 16$ for edge dislocations. Fleischer et al. [17] proposed the value $\alpha = 3$ for Cu alloys as an interaction with screw dislocations while more recent studies by Labusch et al. [18], Gypen et al. [19], and Kratochvíl et al. [33] have found a better correlation with the value $\alpha = 16$, indicating an interaction with edge dislocations.

From the calculation of the hardening parameter, the increase in the critical resolved shear stress (CRSS) due to solid solution strengthening can be inferred and depends on the impurity concentration. In the Fleischer and Labusch model, this relationship has the following form:

$$\tau_{ss} = \frac{1}{Z} \cdot G \cdot \varepsilon^p \cdot c^q \text{ with } \sigma_{ss} = M_T \cdot \tau_{ss} \quad (7)$$

where τ_{ss} is the critical resolved shear stress, and M_T is the Taylor factor with the value of 3.06 for face-centered cubic (fcc) crystal structures, which is generally used as a conversion between the CRSS and yield strength [2,4,34,35]. G is the shear modulus, ε is the hardening parameter, and Z is a solvent-related fitting parameter that varies with the theory used. Furthermore, the exponents p and q vary depending on the theory chosen. Fleischer suggested the values $p = 3/2$ and $q = 1/2$, while Labusch favored $p = 4/3$ and $q = 2/3$. The reason for this is the Fleischer model assumes that the impurity atoms are uniformly distributed along the dislocation line, while Labusch considers a random impurity distri-

bution by introducing a distribution function [18,30]. The model proposed by Fleischer is therefore more suitable for the calculation of substitutionally dissolved impurities in very low concentrations, while the Labusch theory can also be applied to higher impurity concentrations [18,31,36].

3. Materials and Methods

For the experimental investigations, pure copper and binary Cu-Sc alloys with a Sc content in the range of 0.04 to 0.27 wt.% were produced according to the manufacturing process shown in Figure 1. The raw material Cu-OFE and the master alloy CuSc23 were melted using a VC400 casting machine (Indutherm Blue Power Casting Systems, Walzbachtal, Germany) with a 800 g casting weight in a boron-nitride-coated graphite crucible and cast in a preheated graphite mold (with a 10 mm thickness) under vacuum conditions at 1300 °C. In order to ensure a homogeneous microstructure for further experimental investigations and prevent excessive work hardening and potential cracking, the specimens were further processed in two cold-rolling steps with short intermediate annealing. Both rolling stages had an identical logarithmic degree of deformation of $\varphi = 0.6$. The castings were first cold-rolled in the longitudinal direction to a thickness of 5.5 mm. This was carried out on a duo rolling mill (Bühler, Pforzheim, Germany) with 120 mm diameter rolls, which were driven at a speed of 40 min⁻¹. This was followed by short solution annealing for 10 min at 870 °C in a preheated furnace (model ME65/13, Helmut ROHDE GmbH, Prutting, Germany) to minimize impurities. After final rolling to a thickness of 3 mm, the specimens were solution-annealed at 870 °C for 60 min to ensure maximum solubility of scandium in copper and to achieve a fully recrystallized microstructure. Subsequently, the specimens were quenched to room temperature in circulating water.

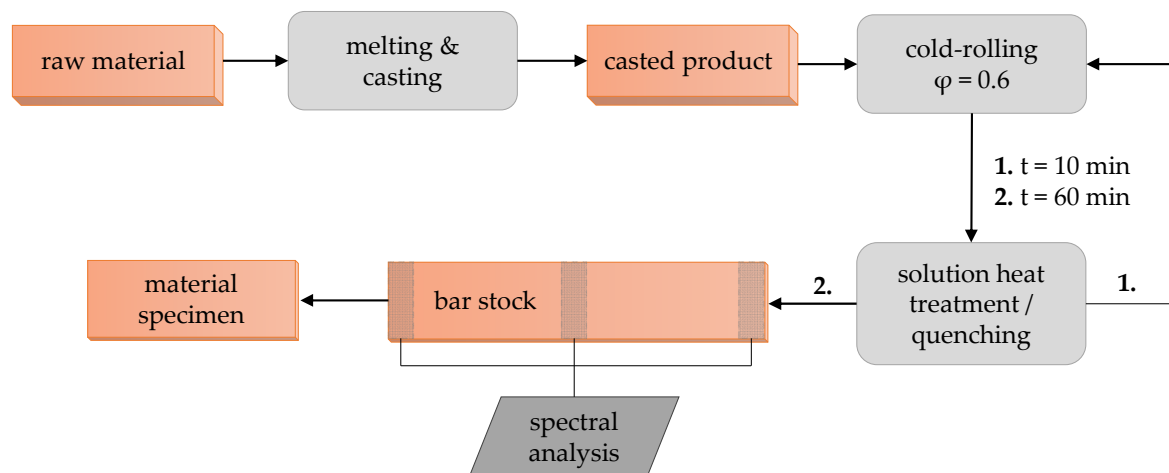


Figure 1. Manufacturing route for the preparation of Cu-OFE and binary Cu-Sc alloys.

After solution annealing, the chemical composition, homogeneity, microstructure, and mechanical properties were examined. In order to avoid possible interactions, the surface layer of the specimens was removed. The content of alloyed scandium was determined at three different points of the rolled and annealed alloy using a calibrated optical emission spectrometer (Spectrotest, SPECTRO Analytical Instruments GmbH, Kleve, Germany) which took eighteen measurements per specimen in total. The maximum deviation from the target composition was 0.02 wt.%. The microstructure characterization was performed with a scanning electron microscope (SEM) (Gemini Sigma VP with the used NTS BSD (Carl Zeiss Microscopy Deutschland GmbH, Oberkochen, Germany)) at 12 kV using a Bruker XFlash 6 | 30 detector (Bruker Nano GmbH, Berlin, Germany).

The mean grain size of the alloys was determined according to the linear intercept method (ASTM E112-13) [37] in five equidistant cross-sections using an optical light microscope (Leica DM ILM LH113, Leica Microsystems, Wetzlar, Germany). For better contrast

in the optical microscope, the specimens were etched according to Klemm III [38]. The examined area was 1.75 cm² and consisted of images of transverse, longitudinal, and ground surfaces for all specimens. The grain boundaries were marked manually. A correction factor $c_{L/D} = 0.79$ was applied to the raw data considering the “tomato salad problem” in spherical stereology [39–41]. The data were approximated using a Gamma distribution, whereby 217–361 chord lengths were marked depending on the specimen.

The electrical conductivity of each specimen was determined using an eddy current test (Sigmascopie SMP10, with TF100A for temperature compensation, Helmut Fischer GmbH, Sindelfingen, Germany) to validate the alloy content. The measurement of electrical conductivity was repeated ten times to minimize errors in the experimental data.

The Vickers hardness test was performed using a microhardness tester (NEXUS 412A, equipped for Vickers hardness testing according to DIN EN ISO 6507-1:2018 [42], Innovatest GmbH, Selkant-Heilder, Germany) with a load of 0.980 N (HV_{0.1}). Seven points were measured for each specimen, and the mean value was calculated to minimize the associated errors.

The mechanical properties were determined by tensile tests (Z100 TEW Allround-Line with VideoXtens biax 2-150 HP for strain measurement; Xforce K 100 kN force measurement system calibrated and verified according to the standards set forth in DIN EN ISO 7500-1 [43]; an accuracy class 1 was achieved for measured forces above 200 N and an accuracy class 0.5 for forces above 1000 N; testXpert III software was used for data evaluation (ZwickRoell GmbH & Co. KG, Ulm, Germany)). The tests were conducted in accordance with the DIN EN ISO 6892-1 [44] traverse-controlled test standard at a test speed of 0.25 mm/min in the elastic area and 8.00 mm/min in the plastic area to determine the yield strength and tensile strength. A minimum of three specimens were tested in tensile tests for each alloy composition. To prevent any potential heat input into the specimens, a cooling water bath was utilized during the milling process. The specified geometry was in close accordance with the specifications set forth in DIN 50125 [45], with a thickness $a_0 = 3$ mm, width $b_0 = 5$ mm, and initial gauge length $l_0 = 17$ mm. For reference, the technical drawing of the tensile specimen geometry is provided in Appendix B, Figure A8.

The specimens were analyzed by X-ray diffraction (XRD) (Seifert XRD 3000TT, Waygate Technologies, Ahrensburg, Germany) in Bragg–Brentano arrangement using CoK_α radiation at 40 kV/40 mA with a scan angle range of 20° to 140° with an increment of 0.05° at a scan speed of 0.15°/min. The lattice parameters were evaluated with the Software Rayflex—analyze (Version 2.503, Waygate Technologies, Ahrensburg, Germany) using a pseudo-Voigt approximation.

The elastic properties of a material were accurately determined using the dynamic resonance method, a non-destructive testing technique (RFDA Basic, IMCE nv, Genk, Belgium). In this method, the resonant frequencies of a specimen are analyzed to determine properties such as Young’s modulus and shear modulus. In this study, specimens measuring 50 × 15 × 3 mm (L × W × H) were subjected to mechanical vibrations using a small hammer. A sensor records the resonant frequencies of these vibrations, which are then analyzed using Fourier analysis. The frequencies were recorded at a sampling rate of 96 kHz, with frequencies below 200 Hz and above 20 kHz excluded from the analysis. The elastic properties could be calculated from the measured frequencies and known material parameters. To minimize experimental errors, at least ten measurements were taken per specimen.

Given the greater relevance of the results to industrial applications, the experimental investigations were correlated with the alloy content’s weight percent, while the modeling was correlated with the atomic fraction in order to facilitate a more comparable analysis of the modeling parameters with other published scientific articles.

With regard to the considerable number of abbreviations, symbols, and indices, a comprehensive overview of these elements is provided in Appendix A, Tables A1–A3.

4. Results

The following chapter presents the results of the investigation of the influence of scandium on the solid solution hardening of the binary Cu-Sc alloy. The chapter is divided into two main sections, covering the experimental investigations and the modeling. Each section provides a comprehensive examination of the experimental results and their implications for understanding the behavior of the alloy.

4.1. Experimental Investigations

4.1.1. Chemical and Microstructural Analysis

The starting point of the investigation was the state of the supersaturated solid solution resulting from quenching it to room temperature after a solution heat treatment. In order to correctly assess the mechanism of solid solution hardening, four Cu-Sc alloys with different compositions were produced. The maximum Sc concentration was 0.27 wt.% and was thus below the maximum solubility of the Cu-Sc of 0.35 wt.%. For the following investigations, the alloys were selected according to the alloy contents listed in Table 1.

Table 1. Compositions in weight percent and atom percent of the experimentally investigated Cu-Sc alloys.

	Sc Content			
at.%	0.06	0.11	0.21	0.39
wt.%	0.04	0.08	0.15	0.27

The homogeneity of the specimens was verified by means of SEM examinations. The investigations using EDX in Appendix A Figure A2 showed that none of the specimens examined exhibited an accumulation of scandium atoms that would indicate a possible second phase besides the Cu crystal. This suggests a homogeneous distribution of Sc atoms in the solid solution.

The electrical conductivity measurements in Figure 2 showed a continuous decrease in electrical conductivity with increasing alloy content. This observation can be attributed to the fact that the electrical resistance increases with the higher concentration of the alloying element [2]. Thus, it can be concluded that the decreasing electrical conductivity is essentially a consequence of solid solution hardening. The measurement of the electrical conductivity for pure copper (Cu-OFE) resulted in a value of 58.7 MS/m, which is in good agreement with the literature value of 58.0 MS/m [6].

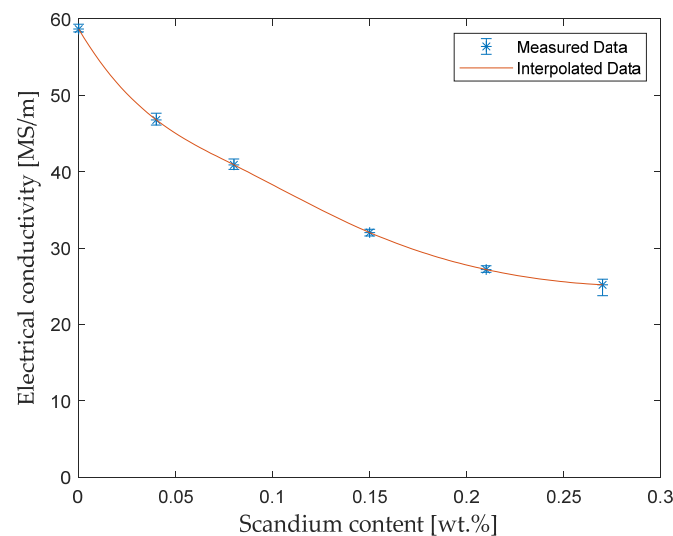


Figure 2. Measured and interpolated data of electrical conductivity of Cu-OFE and Cu-Sc alloys.

4.1.2. X-ray Diffraction Analysis

The (unsmoothed) X-ray diffractometer data of all alloys examined are shown in Figure 3. To improve comparability between the specimens, the peak intensities were normalized and shifted along the y -axis. This normalization allows for a direct comparison of the different specimens by equalizing the height differences of the peaks and thus making the relative intensities of the different diffraction maxima comparable. The diagrams show that all peaks correspond to the characteristic reflections of the copper solid solution phase, which has an fcc crystal structure. Particularly noticeable is the dominant peak of the (111) orientation, which is the most pronounced in most of the alloys. In addition, the absence of peaks other than copper is an indication of the absence of a second phase, suggesting that all of the alloys investigated have a single-crystal Cu-fcc structure or homogeneous solid solutions. The consistency of the observed peaks supports the conclusion that no precipitates or second phases are present. With the increasing Bragg–Brentano angle, a broadening of the peaks is observed, indicating splitting by CoK_α and CoK_β reflexes.

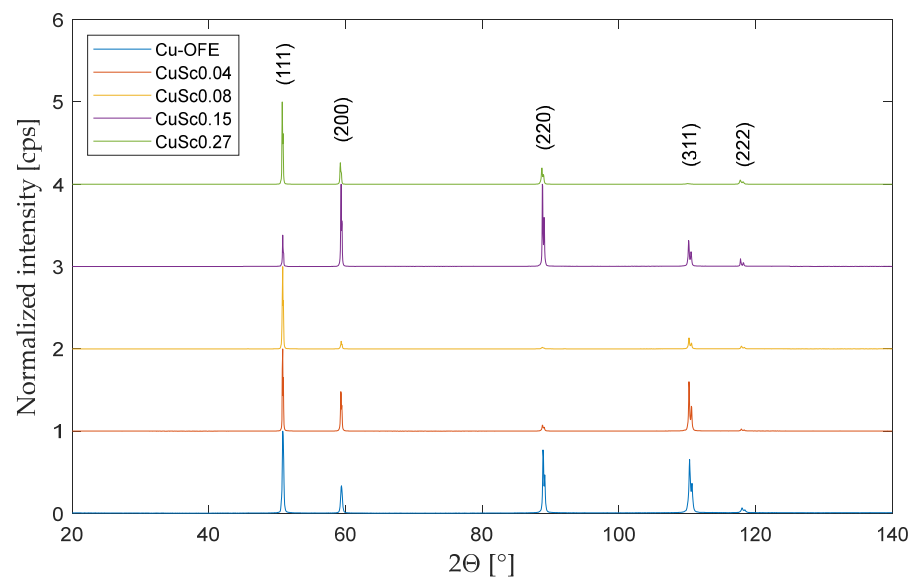


Figure 3. X-ray diffractogram of Cu-OFE and Cu-Sc alloys.

The values of the different Cu-Sc alloys presented in Table 2 demonstrate a clear correlation between the lattice parameters and the scandium content. The lattice parameter determined for pure copper ($a = 3.6146 \text{ \AA}$) is in close agreement with the value reported in the literature ($a = 3.6147 \text{ \AA}$) [46,47]. This substantiates the precision of the conducted measurements and the validity of the experimental techniques employed. As the Sc content increases, the lattice parameter demonstrates a continuous and substantial increase. This indicates a significant interaction between the scandium atoms and the copper matrix, which leads to a widening of the lattice structure. The measurement results illustrate a significant and consistent dependence of the lattice parameter on the scandium concentration in the investigated alloys.

Table 2. Lattice parameters of the experimentally investigated Cu-OFE and Cu-Sc alloys.

Sc content (wt.%)	0.00	0.04	0.08	0.15	0.27
Lattice parameter (\AA)	3.6146	3.6156	3.6171	3.6183	3.6210

4.1.3. Determination of Shear Modulus

The results of the shear modulus measurements obtained using the dynamic resonance method are shown in Table 3, which presents the arithmetic mean of all the conducted measurements. Further experimental data from the dynamic resonance method are provided in

Appendix B, Table A5. It can be seen that the shear modulus increases with increasing Sc content, indicating a higher level of strengthening due to the incorporation of scandium into the Cu matrix. The observed deviations in the measurement results, especially for pure copper, can be attributed to inhomogeneities within the relatively large specimen pieces. For example, these can be caused by local microstructural variations or defects in the material. Despite the variance in the shear modulus values of Cu-OFE in the range of 45.2 to 46.9 GPa, these values show good agreement with the range of values given in the literature of 45.0 to 48.0 GPa [1,6,26,28,46]. The measurement results therefore provide a reliable basis for further analyses and interpretations of the mechanical properties of the alloys investigated.

Table 3. Mean values of shear modulus of the experimentally investigated Cu-OFE and Cu-Sc alloys.

Sc content (wt.%)	0.00	0.04	0.08	0.15	0.27
Shear modulus (GPa)	46.1	46.2	45.9	46.2	46.6

4.1.4. Grain Size Analysis

The grain sizes of the Cu-Sc alloys are shown in Table 4. The mean grain size of the alloys is approximately 300 μm , although there is no clear tendency for the grain size to become finer with increasing alloy content. However, this could also be due to statistical deviations in the approximation of the Gamma distribution, the presence of inclusions or impurities in the specimen, or different temperature or cooling conditions during the heat treatment, which could have an influence on grain growth. A detailed representation of the microstructure obtained by optical light microscopy as well as the (cumulative) distribution density function of the alloys is shown in Appendix B, Figures A3–A7.

Table 4. Mean grain sizes of the experimentally investigated Cu-OFE and Cu-Sc alloys.

Sc content (wt.%)	0.00	0.04	0.08	0.15	0.27
Mean grain size (μm)	301.4	258.2	291.0	338.8	326.6

4.1.5. Tensile Tests

The experimentally determined parameters from tensile tests provide a basis for modeling and predicting the yield strength or CRSS of alloys in conjunction with solid solution hardening. For experimental characterization, the yield strength, defined as the stress at 0.2% plastic strain, was determined. A more detailed overview of additional parameters from the tensile tests is given in Appendix B, Table A4. Table 5 presents the most relevant parameters for the further characterization and classification of the alloys, including the yield strength values $R_{p0.2}$ from the tensile tests, ultimate tensile strength R_m , and elongation at break A . These values are derived from the mean values \bar{x} for each alloy composition, as listed in Appendix B, Table A4. Furthermore, the stress–strain curves for a representative specimen of each alloy composition are provided in Appendix B, Figure A9, for the purpose of facilitating a clear comparison.

Table 5. Mean values of yield strength, ultimate tensile strength, and elongation at break obtained by tensile tests on Cu-OFE and Cu-Sc alloys.

Sc content (wt.%)	0.00	0.04	0.08	0.15	0.27
$R_{p0.2}$ (MPa)	38.8	48.9	57.3	65.8	71.9
R_m (MPa)	203.4	226.9	228.2	236.9	237.7
A (%)	53.9	55.5	54.4	52.8	50.5

It can clearly be seen that both the yield strength and tensile strength increase with increasing alloy content with a significant increase in yield strength from 38.8 MPa to 71.9 MPa between pure copper and CuSc0.27. The tensile strength also increases by 34.3 MPa, which is reflected in a change from approximately 19% (Cu-OFE) up to 30% (CuSc0.27) in relation to the hardening ratio $R_{p0.2}/R_m$. This indicates that alloys with a higher scandium content show a significant increase in strength with a simultaneous decrease in plastic deformability. This is due to strengthening effects caused by the solid solution formation and interaction of the scandium with the copper matrix.

The elongation at break of the materials tested demonstrated a consistent and progressive reduction in value. The initial value of approximately 60% (CuSc0.04) exhibited a gradual decline to reach approximately 50.5% (CuSc0.27). The value for pure copper was approximately 54%, which is situated within the middle range of the measured elongations at break. The experimental values for pure copper (Cu-OFE) are in close agreement with the data given in the literature [46,48]. The results of the investigations indicate that the addition of scandium leads to a reduction in the ductility of the material.

4.2. Modeling

4.2.1. Determination of Strength Increase Due to Solid Solution Hardening

In order to estimate the increase in strength due to the solid solution formation, the influence of grain size on strength was considered. In previous studies by Köster et al. [49] it was found that the Hall–Petch factor k_{HP} is not affected by alloy composition in the course of the increase in strength due to grain size strengthening in copper alloys. It is therefore assumed to remain constant over the range of scandium concentrations investigated here.

The increase in strength due to grain size was determined using the relationship described in Equation (2), the average grain sizes that are given in Table 4, and a Hall–Petch coefficient of $0.14 \text{ MPa} \cdot \sqrt{\text{m}}$. The results of these calculations are visualized in Figure 4.

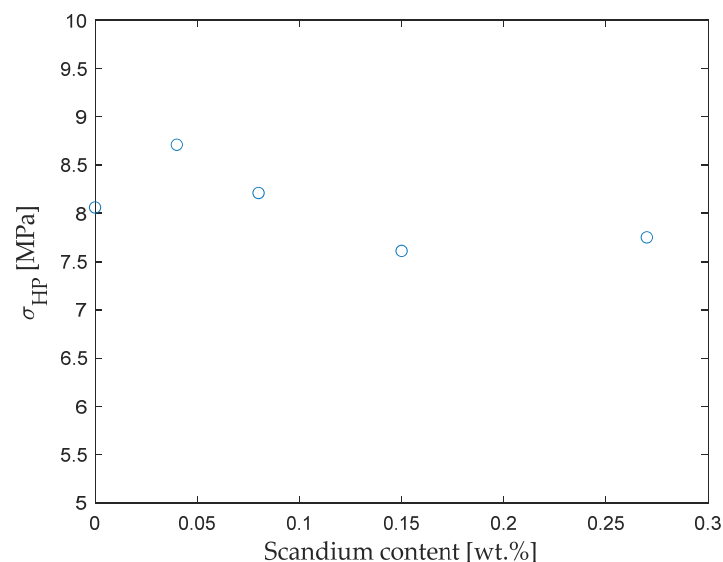


Figure 4. Grain size-dependent strength increase of Cu-OFE and Cu-Sc alloys.

Figure 4 shows the effect of grain size on the strength of pure copper and Cu-Sc alloys. It can be seen that the increase in strength due to grain size is averaged to be about 8 MPa.

Figure 5 shows the measured yield strengths and the corrected values for the grain size-related strength contribution. Grain size was found to have an effect of approximately 21% on the overall strength of the pure copper.

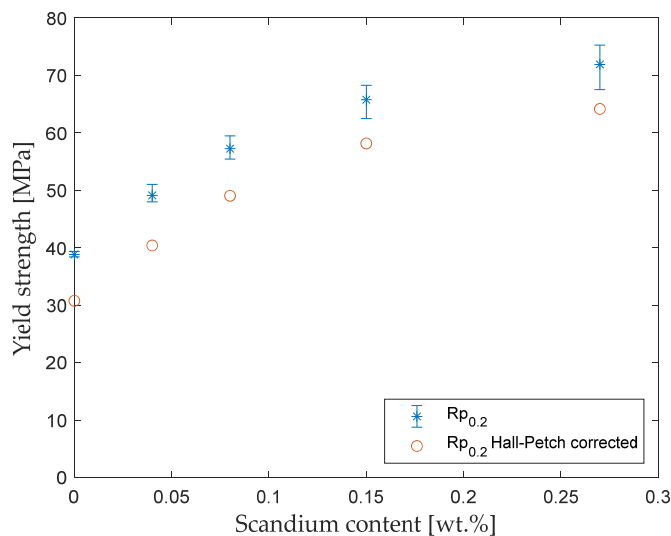


Figure 5. Measured and Hall–Petch corrected yield strength data of Cu-OFE and Cu-Sc alloys.

Based on the analyses carried out in Sections 4.1.1 and 4.1.2, precipitation strengthening can be neglected as a further strengthening mechanism as no second phase was detected. Given that all of the alloys were produced in the same way, a simplifying assumption for further calculations can be made that the strength contribution due to dislocations σ_{dis} is identical in all of the alloys. It can therefore be concluded that the increase in strength with increasing scandium concentration is exclusively due to the mechanism of solid solution hardening. From the fact that there is no increase in strength due to the solid solution in the pure copper, the following relationship can be applied:

$$\sigma_0 = \sigma_{y(Cu-OFE)} - \sigma_{HP(Cu-OFE)} = 30.77 \text{ MPa} \tag{8}$$

In this context, the intrinsic strength σ_0 represents the hypothetical material’s strength, where the influence of solid solution strengthening and grain boundary effects is not considered. The following relationship can be derived from Equations (1) and (8) for the further modeling of all of the alloys considered:

$$\sigma_{ss} = \sigma_y - \sigma_{HP} - \sigma_0 \tag{9}$$

The results of the calculations are shown in Table 6.

Table 6. Estimated solid solution strengthening.

Sc content (wt.%)	0.00	0.04	0.08	0.15	0.27
σ_{ss} (MPa)	0.00	9.47	18.12	27.23	33.24

4.2.2. Determination of Parelastic and Dielastic Misfit Parameter

To determine the parelastic and dielastic misfit parameters, the changes in lattice parameter and shear modulus due to the alloying of scandium were extracted from the available experimental studies in Tables 2 and 3. First, a linear regression was performed. The values da/dc and dG/dc were determined separately using the lattice parameter change (Equation (3)) and the shear modulus change (Equation (4)). To ensure comparability with other solid solution hardening studies, the measured values were plotted as a function of the scandium concentration in atomic percentage. The experimentally determined values of the lattice parameters (Figure 6a) and the shear moduli (Figure 6b) are shown below along with their linear correlation.

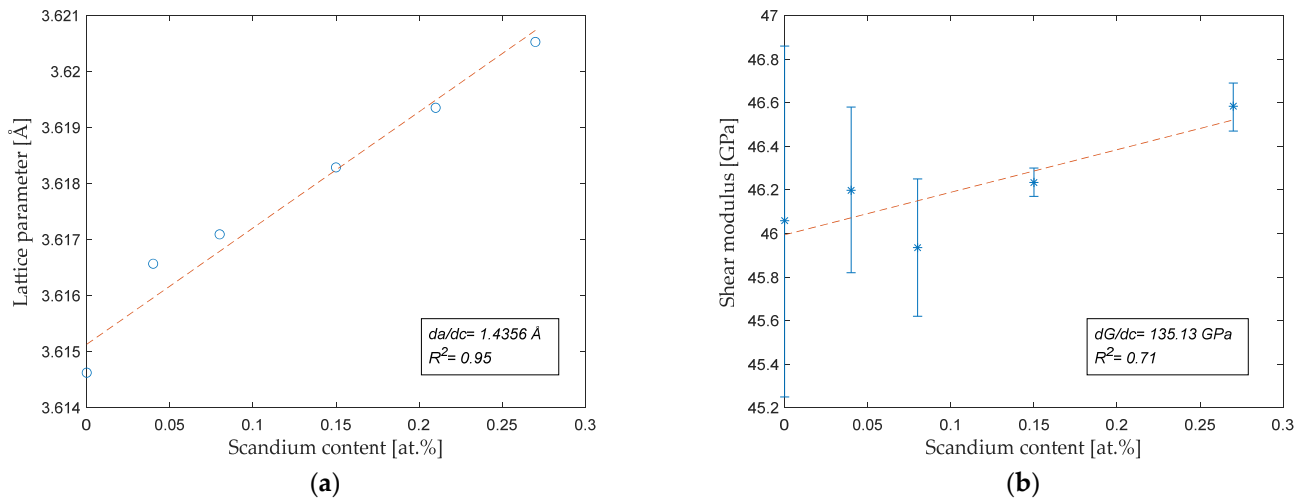


Figure 6. Experimentally measured values (blue) as a function of the Sc content and their approximated linear change with the alloy concentration in atomic percentage (red): (a) Lattice parameter; (b) Shear modulus.

As illustrated in Figure 6a, the linear correlation (da/dc) of the lattice parameter demonstrates a change of 1.4356 Å, with a Pearson correlation coefficient of $R^2 = 0.95$. This indicates a strong linear relationship between the change in the lattice parameter and the concentration of alloying atoms. In contrast, the shear modulus correlation (dG/dc) in Figure 6b demonstrates a change of 135.13 GPa, though with a lower level of accuracy reflected in its R^2 value of 0.71. The base values of the lattice parameter (a) and shear modulus (G) are derived from the y-intercepts of the regression. Based on the available data, the parelastic misfit parameter δ and the elastic misfit parameters η' and η_{GD} now can be determined using Equations (3)–(5). The results are given in Tables 7 and 8. The dependence of the shear modulus on lattice contraction/expansion caused by dissolved atoms, as proposed by Gypen et al., leads to an increase in the misfit parameter by a value of 0.23 compared to the classical Labusch theory.

Table 7. Dielastic and modified dielastic misfit parameters used for modeling.

G (GPa)	dG/dc (GPa)	η	η'	η_{GD}
46.00	135.13	2.94	1.19	1.42

Table 8. Parelastic misfit parameters used for modeling.

a (Å)	da/dc (Å)	δ
3.6151	1.4356	0.3971

The results of these calculations yield the hardening parameters ϵ , which are presented in Table 9. The hardening parameters ϵ_{Fl} and ϵ_{La} were determined using the corresponding Fleischer and Labusch theories, as defined in Equation (6), with consideration of the misfit parameters δ and η' . The hardening parameter ϵ_{La-GD} corresponds to the parameter calculated according to the Labusch theory but using the misfit parameter η_{GD} proposed by Gypen et al.

Table 9. Hardening parameters according to theories of Fleischer adapted from Ref. [17], Labusch adapted from Ref. [18], and Labusch with Gypen misfit parameter adapted from Ref. [19].

ϵ_{Fl}	ϵ_{La}	ϵ_{La-GD}
7.544	6.464	6.511

By utilizing the weighting parameter $\alpha = 16$, as recommended by Labusch et al. [18], Gypen et al. [19], and Kratochvíl et al. [33], the impact of the dielastic effect can be significantly minimized. As a result, the hardening parameter $\epsilon_{\text{La-GD}}$ is observed to exhibit a negligible difference from that of the classical Labusch approach. The correlation analysis between the modelled hardening parameters and experimental data from the tensile tests was performed using several parameters. Figure 7 presents the experimental values and modelled curves according to the different theories. The findings revealed that the best fit with the experimental data was achieved with the fitting parameters $Z_{\text{La}} = 1160$ and $Z_{\text{Fl}} = 5400$, when the respective theories were applied. Conversely, the largest discrepancies between the modelled and the experimental values were observed for the strength values of CuSc0.04 and CuSc0.27. Nonetheless, the correlations resulted in a Pearson correlation coefficient of $R^2_{\text{Fl}} = 0.90$ when applying the Fleischer theory and $R^2_{\text{La}} = R^2_{\text{La-GD}} = 0.94$ when applying the Labusch theory.

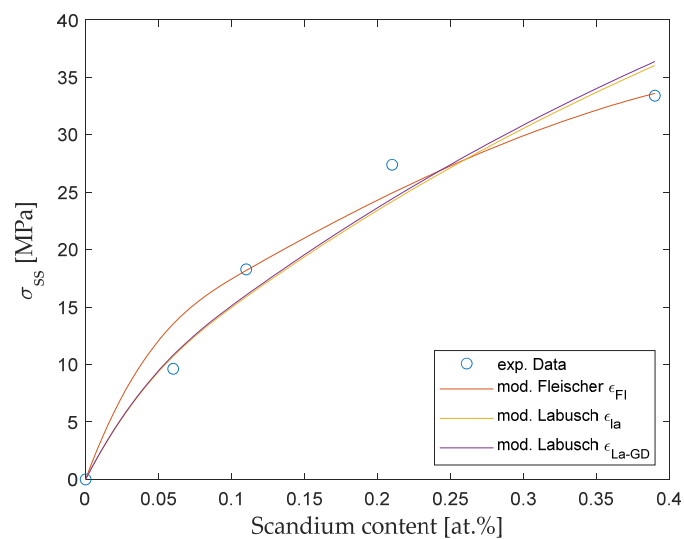


Figure 7. Experimentally determined increase in strength due to solid solution hardening and strength modelled according to theories of Fleischer adapted from Ref. [17], Labusch adapted from Ref. [18], and Labusch with Gypen misfit parameter adapted from Ref. [19].

5. Discussion

The influence of scandium dissolved in copper on its strength is found to be significant in the analyzed alloy range. Scandium contents of up to 0.39 at.% result in a clearly measurable change in the lattice parameter due to large differences in atomic size. An increase in the shear modulus with increasing scandium content is observed. The empirical increase in strength as a function of the alloy content (in the atomic fraction) is $\sigma_{ss}/dc^{1/2} = 542.75$ MPa and $\sigma_{ss}/dc^{2/3} = 1557.30$ MPa. This corresponds to a considerable increase in strength compared to that of the other alloying elements in copper. A comparison with the other alloying elements shows that the hardening parameter ϵ_{La} exhibits a significant above-average increase, as illustrated in Figure 8. The change in critical resolved shear stress (CRSS) per atomic fraction was visualized according to the Labusch model with the weighting parameter $\alpha = 16$ in relation to the hardening parameter ϵ_{La} .

With regard to the misfit parameters, it can be seen that the misfit parameter η_{GD} , as proposed by Gypen et al., differs significantly from the Labusch parameter. This discrepancy is due to the additional effects of lattice distortion that Gypen et al. consider. However, when both parameters are employed in the formula proposed by Labusch for calculating the hardening parameter, the effect is minimal. This is due to the fact that the shear modulus exerts a very small influence with regard to edge dislocations, which interact strongly with impurity atoms that have an isotropic distortion field. The influence of the weighting parameter α significantly reduces the influence of the dielastic parameter.

Zhang et al. [51] conducted studies in which they performed ab initio calculations to determine the mechanism of solid solution hardening using the Labusch theory in copper alloys. Their results indicate that scandium has a particularly high potential for solid solution strengthening in copper. However, their calculations indicate a reduction in the shear modulus with increasing scandium content with a value of $dG/dc = -130.30$ GPa. Given that the dielastic misfit parameter is quadratic in the equation of the hardening parameter of the Labusch equation, this results in only a minor change in the hardening effect compared to the measurements presented here. Nevertheless, the actual effect of the change in shear modulus in the solid solution can be considered to be very small. Should the modification of the shear modulus not be considered in this instance, where η is set to 0, the resulting impact on the material's strength would be a decline of -0.80 MPa when utilizing identical parameters at a scandium concentration of 0.27 wt.%; this result is within the measured uncertainty detailed in Table A4.

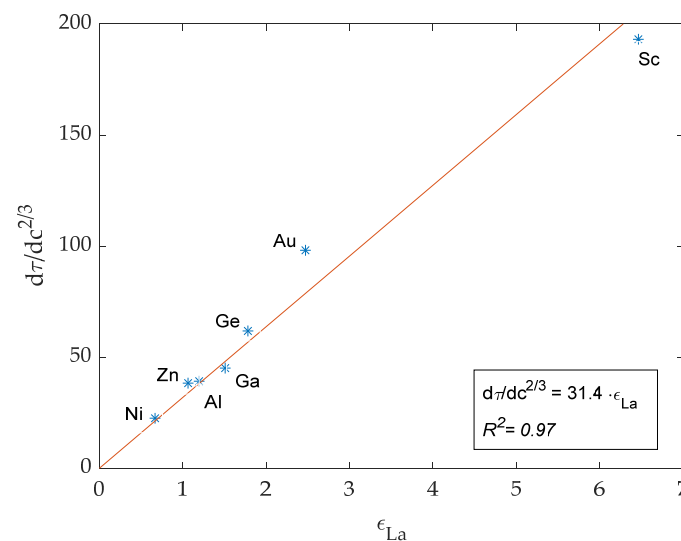


Figure 8. Correlation of hardening parameter ϵ_{La} and $d\tau/dc^{2/3}$ according to Labusch theory for various Cu alloys adapted from Refs. [19,33,50] and Cu-Sc alloys (this study).

Zhang et al. [51] estimated a misfit parameter of 0.2707 for the parelastic effect, which is significantly lower compared to the value of 0.3971 exhibited by the experimental results presented here. Previous studies investigating solid solution hardening have indicated that the Labusch model offers a more accurate representation than the Fleischer model [19,33,36,52]. This was confirmed with the alloys investigated here, although a good level of agreement was also achieved with the Fleischer model. In this study, the fitting parameter Z_{La} was found to have a value of 1160, which correlates well with the values reported by Jax et al. [52] and Kratchovíl et al. (1250 for both), who investigated the effect of various alloying elements (Al, Zn, Ga, Ge, and Au) on the hardening of copper.

6. Conclusions

The objective of this investigation was to analyze the dielastic and parelastic effects that determine the mechanism of solid solution hardening for Sc in Cu. The effects were investigated through the utilization of the dynamic resonance methodology to assess the elastic properties and X-ray diffraction techniques to ascertain the lattice constants of the alloys. Furthermore, a correlation of the results with experimental investigations of the yield strength was investigated using the common theories of Fleischer and Labusch, along with the quantification of solid solution hardening of copper–scandium alloys. The outcomes of the computations and measurements yielded the following conclusions:

- The influence of scandium dissolved in copper on the strength is significant in the investigated alloy range up to 0.27 wt.%, leading to an increase in strength of approximately 33 MPa;
- The main strength-increasing mechanism is the parastic effect of lattice distortion, which is caused by atomic size differences between copper and scandium;
- The enhancement in strength resulting from the solid solution hardening of scandium in copper can be attributed to both Fleischer's and Labusch's theories. However, the correlation between the observed phenomenon and the Labusch theory is more pronounced than that observed with the Fleischer theory. This observation is consistent with other published findings.

In the present study, the maximum addition of scandium in copper was 0.27 wt.%, which is below the reported solubility limit of 0.35 wt.%. To gain further insight into the limits of solid solution strengthening, it would be beneficial to conduct further studies with increased scandium concentrations. The results presented indicate the potential for the further strengthening of Cu-Sc alloys. With the maximum solubility of 0.35 wt.%, an increase in strength of up to 38.0–42.4 MPa compared to pure copper can be expected with the model parameters presented here.

However, micro-alloyed Cu alloys are primarily considered for industrial applications that require high levels of electrical conductivity and high levels of strength. Despite the notable enhancement in strength, the dissolution of scandium in the solid solution leads to a considerable reduction in electrical conductivity. In order to achieve both high levels of hardness and electrical conductivity, the precipitation hardening of the Cu-Sc alloy is of great importance for future research. Modeling this phenomenon would be highly valuable in assessing the competitiveness of Cu-Sc alloys compared to industrial alloys such as Cu-Cr or Cu-Zr, which are frequently used in this field of application. Moreover, the influence of additional alloying elements may yield potential synergistic effects on the strengthening mechanisms.

Author Contributions: Conceptualization, R.H.; methodology, R.H.; validation, R.H. and S.K.; formal analysis, R.H. and G.N.; investigation, R.H., S.K. and N.J.; resources, R.H., J.D. and A.Z.; data curation, R.H.; writing—original draft preparation, R.H.; writing—review and editing, S.K., N.J., G.N., A.Z., J.D. and U.P.; visualization, R.H.; supervision, G.N., A.Z. and U.P. All authors have read and agreed to the published version of the manuscript.

Funding: This research received no external funding.

Data Availability Statement: The original contributions presented in the study are included in the article, further inquiries can be directed to the corresponding author.

Acknowledgments: The authors would like to thank Thomas Hersacher (Cooperative State University Heidenheim) and Ruben Krampulz (Cooperative State University Stuttgart) for their technical support in the preparation of the copper–scandium alloy test specimens.

Conflicts of Interest: The authors declare no conflicts of interest.

Appendix A

Table A1. List of abbreviations.

Abbreviation	Description
BSD	Back scatter detector
CDF	Cumulative distribution function
Cr	Chromium
Cu	Copper
Cu-OFE	Oxygen-free and non-phosphorus-deoxidized copper (Oxygen Free Electronic Grade) with a guaranteed purity of 99.99%
CRSS	Critical resolved shear stress

Table A1. Cont.

Abbreviation	Description
EDX	Energy dispersive X-ray spectroscopy
fcc	Face-centered cubic
PDF	Probability density function
SEM	Scanning electron microscope
SGTE	Scientific Group Thermodata Europe
Sc	Scandium
XRD	X-ray diffraction
Zr	Zirconium

Table A2. List of symbols.

Symbol	Unit	Description
a	$\text{\AA} = \text{m}^{-10}$	Lattice parameter
A	-	Fitting parameter, with $A = 5$ for Cu alloys
A	%	Elongation at break
A_g	%	Uniform extension
α	-	Weighting parameter
a_0	mm	Thickness of tensile specimens
b_0	mm	Width of tensile specimens
c	-	Atom fraction/mass fraction
d	μm	Grain size
δ	-	Parelastic interaction parameter
E	GPa	Young's modulus
ε	-	Hardening parameter
G	GPa	Shear modulus
H	HV _{0.1}	Hardness
μ	-	Poisson ratio
η	-	Modulus parameter
H'	-	Modified modulus parameter
k_{HP}	$\text{MPa} \cdot \sqrt{\text{m}}$	Hall–Petch constant
l_0	mm	Initial gauge length of tensile specimens
M_T	-	Taylor factor ($M_T = 3.06$ for fcc)
p	-	Exponent
q	-	Exponent
$R_{p0.2}$	MPa	Yield strength at 0.2% plastic strain
R_m	MPa	Ultimate tensile strength
R^2	-	Pearson correlation coefficient
φ	-	Logarithmic degree of deformation
s	-	Standard deviation
σ	S/m	Electrical conductivity
σ	MPa	Stress
τ	MPa	Critical resolved shear stress
W_B	J	Fracture energy
\bar{x}	-	Arithmetic mean value
Z	-	Fitting parameter

Table A3. List of indices.

Index	Description
dis	Dislocation
Fl	Fleischer
GD	Gypen–Deruyttere
HP	Hall–Petch
La	Labusch
La-GD	Combination of Labusch theory with misfit parameter proposed by Gypen et al.
p	Precipitation
ss	Solid solution
y	Yield strength
0	Intrinsic

Appendix B

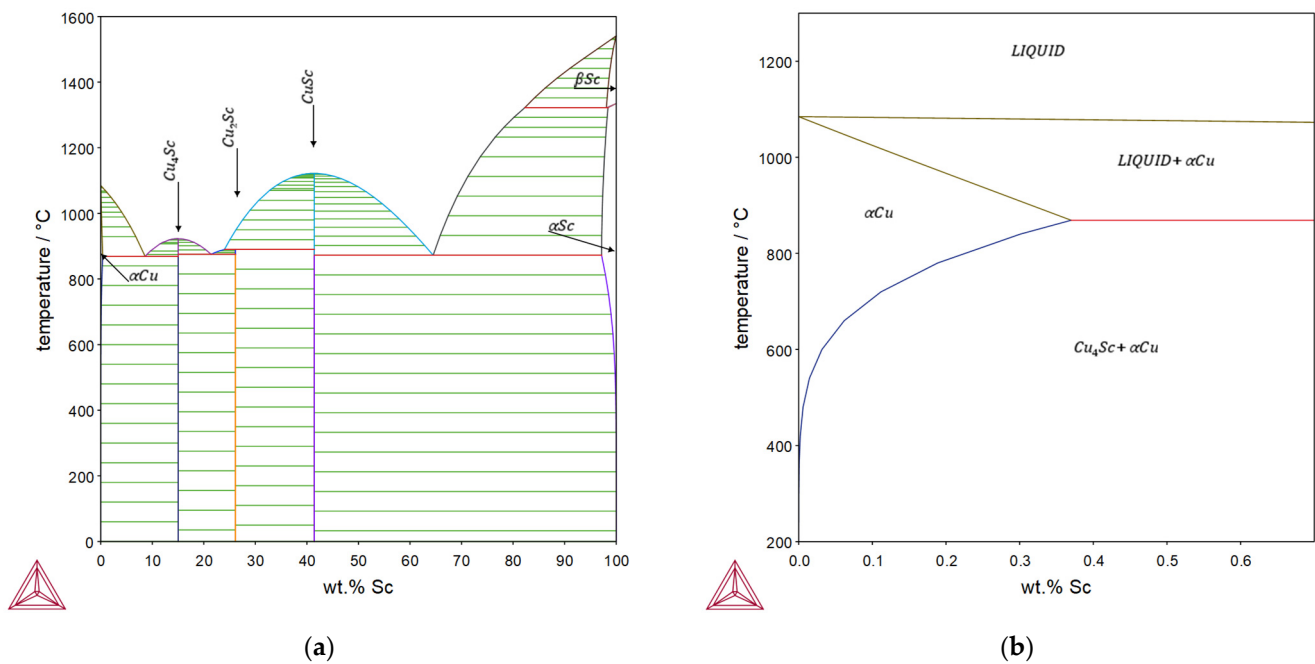


Figure A1. Phase diagram of the binary copper–scandium system calculated with the Thermo-Calc SGTE database (2022a): (a) overall; (b) copper-rich area reprinted from Ref. [8].

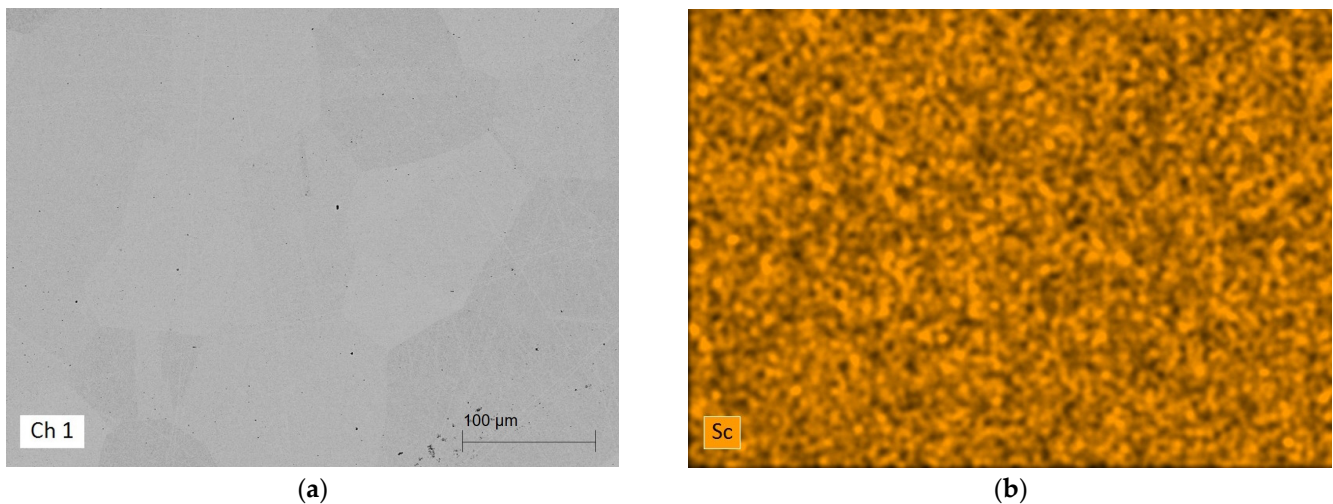


Figure A2. Homogeneous distribution of the alloying element scandium after a 60 min solution heat treatment at 870 °C, analyzed with EDX: (a) backscatter detection; (b) EDX distribution of Sc.

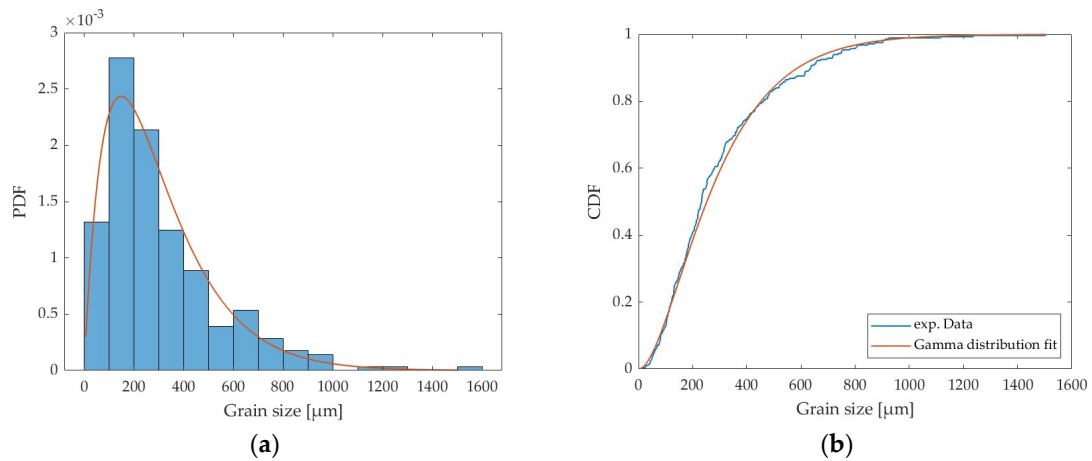


Figure A3. Experimentally determined grain size distribution (blue) approximated with Gamma distribution (red) of the solution-annealed XRD specimens for Cu-OFE: (a) probability density function (PDF); (b) cumulative distribution function (CDF).

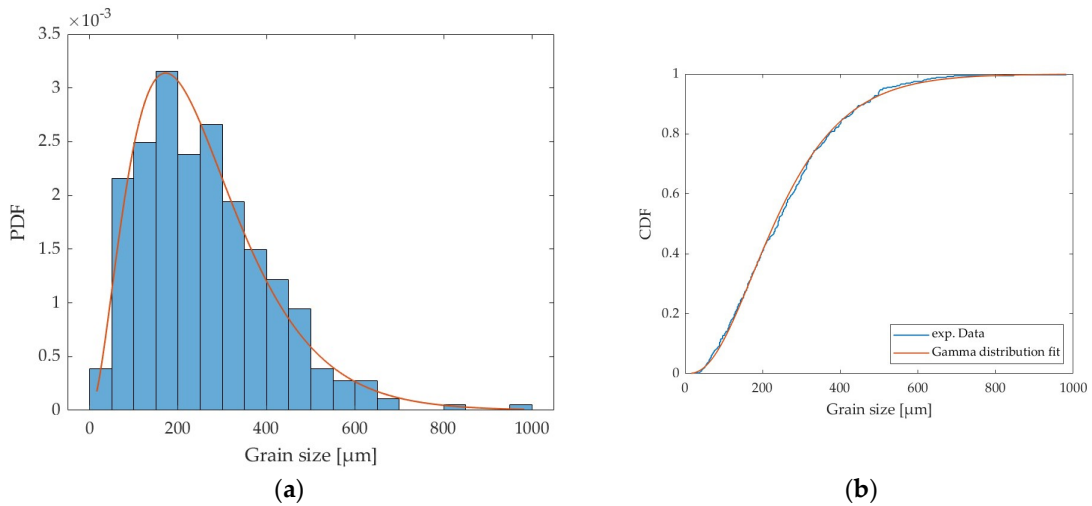


Figure A4. Experimentally determined grain size distribution (blue) approximated with Gamma distribution (red) of the solution-annealed XRD specimens for CuSc0.04: (a) probability density function (PDF); (b) cumulative distribution function (CDF).

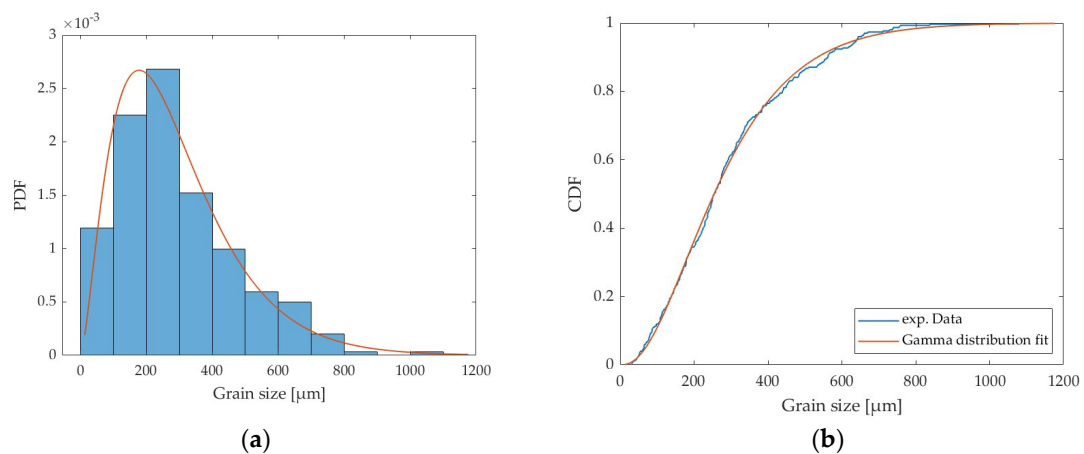


Figure A5. Experimentally determined grain size distribution (blue) approximated with Gamma distribution (red) of the solution-annealed XRD specimens for CuSc0.08: (a) probability density function (PDF); (b) cumulative distribution function (CDF).

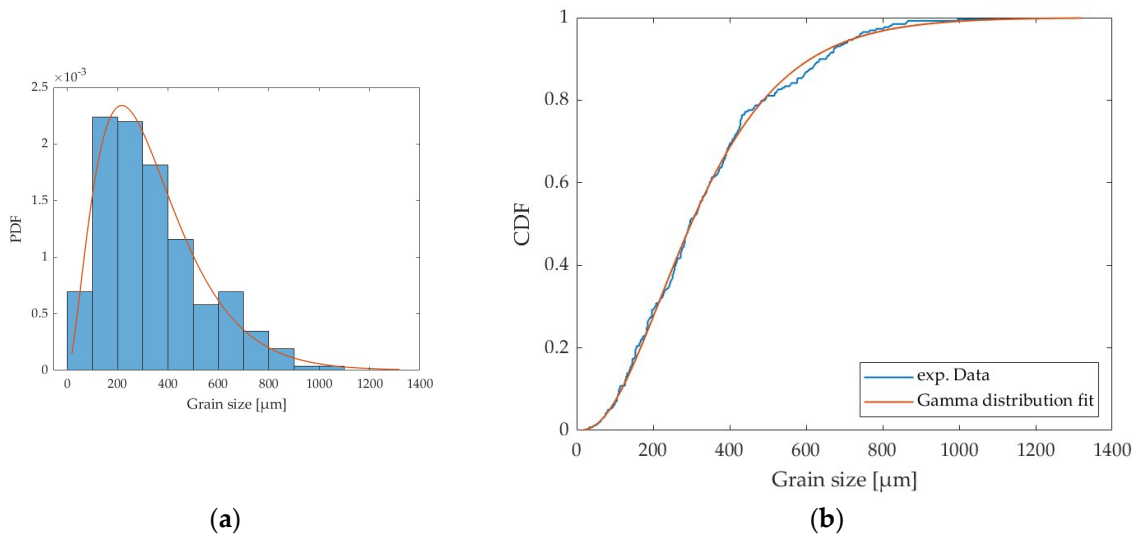


Figure A6. Experimentally determined grain size distribution (blue) approximated with Gamma distribution (red) of the solution-annealed XRD specimens for CuSc0.15: **(a)** probability density function (PDF); **(b)** cumulative distribution function (CDF).

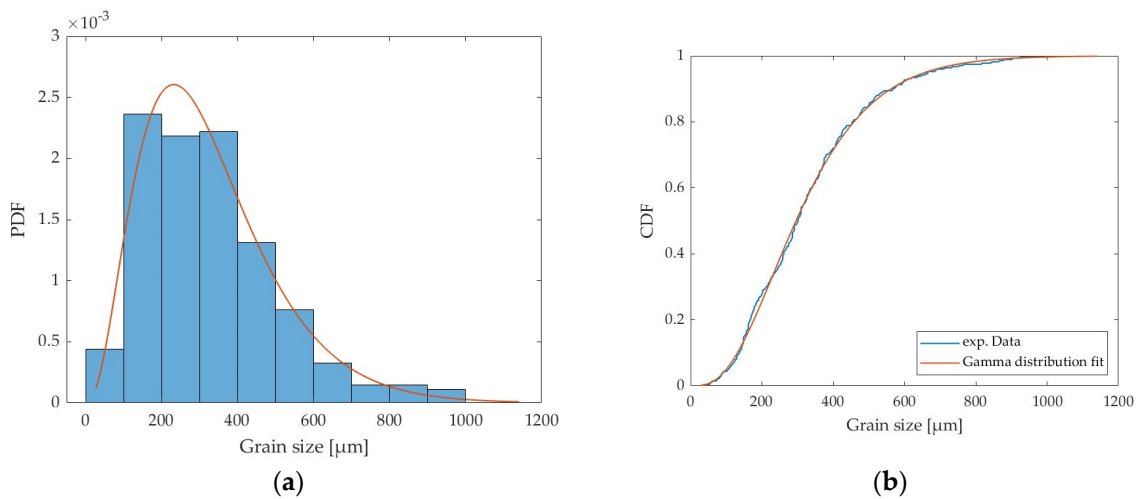


Figure A7. Experimentally determined grain size distribution (blue) approximated with Gamma distribution (red) of the solution-annealed XRD specimens for CuSc0.27: **(a)** probability density function (PDF); **(b)** cumulative distribution function (CDF).

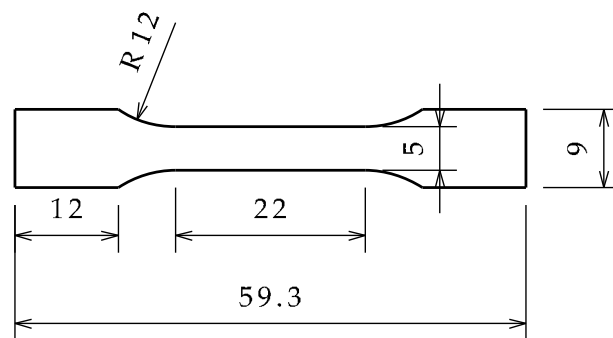


Figure A8. Technical drawing of the tensile specimen dimensions (unit: mm) used in the study, according to DIN 50125 [45].

All relevant parameters from the valid tensile tests and those obtained using the dynamic resonance method in the solution-annealed condition of pure copper (Cu-OFE) and the Cu-Sc alloys were recorded as part of this study. The stress–strain curves presented in Figure A9 are based on one representative specimen per alloy composition from the valid tensile tests. More detailed information regarding the tensile tests can be found in Table A4, while the measurements obtained using the dynamic resonance method are detailed in Table A5. The mean value of all valid measurements is denoted by \bar{x} , and the standard deviation by s .

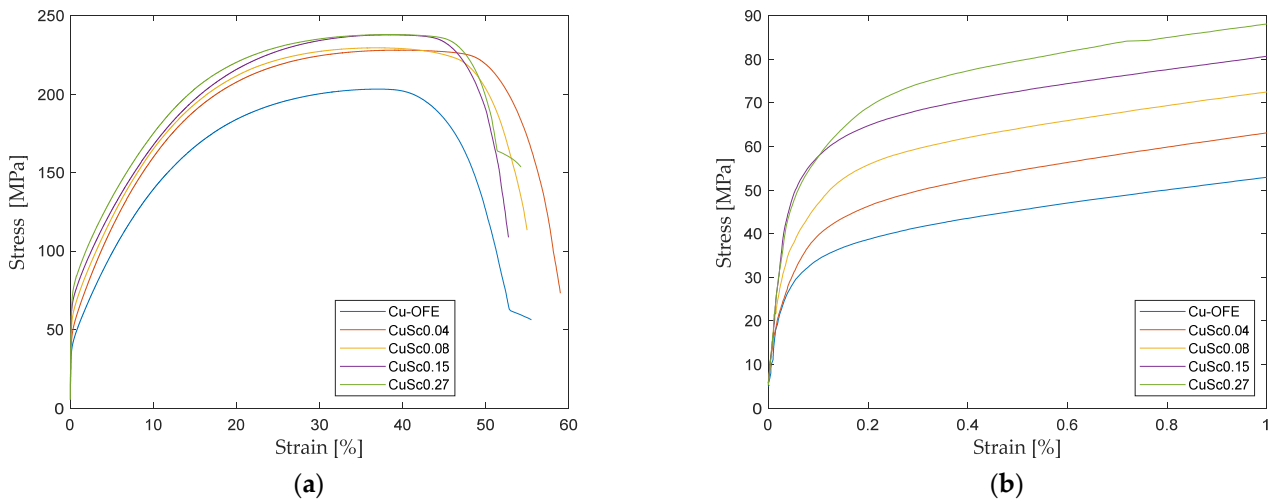


Figure A9. Stress–strain curves of tensile tests for Cu-OFE and Cu-Sc alloys: (a) overall view; (b) enlarged view up to 1% strain.

Table A4. Measurements of relevant parameters of tensile tests for Cu-OFE and Cu-Sc alloys.

Sc Content (wt.%)	Specimen Number	E (GPa)	$R_{p0.2}$ (MPa)	R_m (MPa)	$R_m/R_{p0.2}$ (%)	A (%)	A_g (%)	μ (-)	W_B (J)
0.00	1	114.4	38.4	203.6	18.9	52.3	35.6	0.4	20.9
	2	68.0	38.7	203.4	19.0	54.0	38.8	0.4	22.8
	3	53.7	39.4	203.2	19.4	55.5	36.7	0.4	21.6
	\bar{x}	78.7	38.8	203.4	19.1	53.9	37.0	0.4	21.8
	s	25.9	0.4	0.1	0.2	1.3	1.3	0.0	0.8
0.04	1	72.9	48.2	224.3	21.5	51.3	37.1	0.4	23.4
	2	47.2	48.3	227.1	21.3	60.7	39.5	0.4	27.9
	3	97.6	48.0	228.0	21.0	58.9	39.8	0.4	28.1
	4	104.6	51.0	228.1	22.4	51.2	36.7	0.4	24.1
	\bar{x}	80.6	48.9	226.9	21.5	55.5	38.3	0.4	25.9
s	22.6	1.3	1.5	0.5	4.3	1.4	0.0	2.2	
0.08	1	90.4	55.4	227.1	24.4	58.2	39.4	0.4	27.7
	2	88.2	57.1	229.5	24.9	54.9	37.1	0.3	26.4
	3	103.7	57.0	227.6	25.1	56.3	36.9	0.4	25.5
	4	76.5	59.5	228.7	26.0	48.1	35.8	0.3	22.1
	\bar{x}	89.7	57.3	228.2	25.1	54.4	37.3	0.3	25.4
s	9.7	1.4	0.9	0.6	3.8	1.3	0.0	2.1	
0.15	1	104.8	62.5	234.9	26.6	55.7	38.4	0.4	26.4
	2	115.9	66.8	237.8	28.1	52.6	38.1	0.3	26.3
	3	110.6	68.3	239.1	28.6	52.0	36.2	0.4	25.2
	4	79.9	65.5	235.7	27.8	50.9	36.1	0.3	24.0
	\bar{x}	102.8	65.8	236.9	27.8	52.8	37.2	0.3	25.5
s	13.8	2.1	1.7	0.7	1.8	1.1	0.0	1.0	

Table A4. Cont.

Sc Content (wt.%)	Specimen Number	E (GPa)	R _{p0.2} (MPa)	R _m (MPa)	R _m /R _{p0.2} (%)	A (%)	A _g (%)	μ (-)	W _B (J)
0.27	1	90.1	75.3	237.2	31.7	53.5	38.5	0.4	26.5
	2	126.4	72.2	238.0	30.3	54.1	37.9	0.4	27.0
	3	105.0	72.7	234.9	30.9	45.8	34.9	0.4	22.3
	4	96.7	67.5	240.6	28.1	48.7	34.5	0.4	24.2
	\bar{x}	104.5	71.9	237.7	30.3	50.5	36.5	0.4	25.0
	s	13.7	2.8	2.0	1.4	3.5	1.8	0.0	1.9

Table A5. Measurements of relevant parameters using dynamic resonance method for Cu-OFE and Cu-Sc alloys.

Sc Content (wt.%)		Specimen Measurement											
		1	2	3	4	5	6	7	8	9	10	\bar{x}	s
0.00	E [GPa]	117.3	117.3	117.3	117.1	117.1	125.1	125.2	125.0	125.1	125.0	121.1	4.0
	G [GPa]	45.2	45.5	45.2	45.2	45.2	46.9	46.9	46.9	46.9	46.8	46.1	0.8
	μ [-]	0.3	0.3	0.3	0.3	0.3	0.3	0.3	0.3	0.3	0.3	0.3	0.0
0.04	E [GPa]	129.0	129.0	128.9	129.0	129.0	129.8	129.8	129.8	129.8	129.8	129.4	0.4
	G [GPa]	46.6	46.6	46.6	46.6	46.6	45.8	45.8	45.8	45.8	45.8	46.2	0.4
	μ [-]	0.4	0.4	0.4	0.4	0.4	0.4	0.4	0.4	0.4	0.4	0.4	0.0
0.08	E [GPa]	126.4	126.4	126.4	126.4	126.4	127.0	127.0	127.0	127.0	127.0	126.7	0.3
	G [GPa]	46.3	46.3	46.3	46.3	46.3	45.6	45.6	45.6	45.6	45.6	45.9	0.3
	μ [-]	0.4	0.4	0.4	0.4	0.4	0.4	0.4	0.4	0.4	0.4	0.4	0.0
0.15	E [GPa]	123.9	123.9	123.9	123.9	123.9	126.7	126.7	126.7	126.7	126.7	125.3	1.4
	G [GPa]	46.2	46.2	46.2	46.2	46.2	46.3	46.3	46.3	46.3	46.3	46.2	0.1
	μ [-]	0.3	0.3	0.3	0.3	0.3	0.4	0.4	0.4	0.4	0.4	0.4	0.0
0.27	E [GPa]	122.9	122.9	122.9	122.9	122.9	124.9	124.8	124.9	124.9	124.9	123.9	1.0
	G [GPa]	46.7	46.7	46.7	46.7	46.7	46.5	46.5	46.5	46.5	46.5	46.6	0.1
	μ [-]	0.3	0.3	0.3	0.3	0.3	0.3	0.3	0.3	0.3	0.3	0.3	0.0

References

- Davis, J.R. (Ed.) *Copper and Copper Alloys*, 2nd ed.; ASM International: Materials Park, OH, USA, 2008; ISBN 9780871707260.
- Gottstein, G. *Materialwissenschaft und Werkstofftechnik: Physikalische Grundlagen*; Springer: Berlin/Heidelberg, Germany, 2014; ISBN 978-3-642-36602-4.
- Roos, E.; Maile, K.; Seidenfuß, M. *Werkstoffkunde für Ingenieure: Grundlagen, Anwendung, Prüfung*; Springer: Berlin/Heidelberg, Germany, 2017; ISBN 9783662495322.
- Hornbogen, E.; Warlimont, H.; Skrotzki, B. (Eds.) *Metalle*; Springer: Berlin/Heidelberg, Germany, 2019; ISBN 978-3-662-57762-2.
- Haasen, P. *Physikalische Metallkunde*; Reprint 2021; De Gruyter: Berlin/Heidelberg, Germany; Boston, MA, USA, 2022; ISBN 9783112569702.
- Dies, K. *Kupfer und Kupferlegierungen in der Technik*; [Auflage 1967]; Springer: Berlin/Heidelberg, Germany, 2014; ISBN 978-3-642-48932-7.
- Franczak, K.; Kwaśniewski, P.; Kiesiewicz, G.; Zasadzińska, M.; Jurkiewicz, B.; Strzypek, P.; Rdzawski, Z. Research of mechanical and electrical properties of Cu–Sc and Cu–Zr alloys. *Archiv. Civ. Mech. Eng.* **2020**, *20*, 28. [[CrossRef](#)]
- Dölling, J.; Henle, R.; Prah, U.; Zilly, A.; Nandi, G. Copper-Based Alloys with Optimized Hardness and High Conductivity: Research on Precipitation Hardening of Low-Alloyed Binary CuSc Alloys. *Metals* **2022**, *12*, 902. [[CrossRef](#)]
- Arzhavitin, V.M.; Korotkova, I.M.; Sytin, V.I. Grain-boundary internal friction of yttrium- or scandium-microalloyed copper. *Russ. Metall.* **2016**, *2016*, 229–234. [[CrossRef](#)]
- Henle, R.; Dölling, J.; Prah, U.; Nandi, G.; Zilly, A. DSC Analysis of the Effect of Cold Deformation on the Precipitation Kinetics of a Binary Cu-Sc Alloy. *Materials* **2023**, *16*, 3462. [[CrossRef](#)]
- Dölling, J.; Kracun, S.F.; Prah, U.; Fehlbier, M.; Zilly, A. A Comparative Differential Scanning Calorimetry Study of Precipitation Hardenable Copper-Based Alloys with Optimized Strength and High Conductivity. *Metals* **2023**, *13*, 150. [[CrossRef](#)]
- Bo, H.; Liu, L.B.; Jin, Z.P. Thermodynamic analysis of Al–Sc, Cu–Sc and Al–Cu–Sc system. *J. Alloys Compd.* **2010**, *490*, 318–325. [[CrossRef](#)]
- Subramanian, P.R.; Laughlin, D.E.; Chakrabarti, D.J. The Cu-Sc (copper-scandium) system. *Bull. Alloy Phase Diagr.* **1988**, *9*, 378–382. [[CrossRef](#)]

14. Goncharuk, L.V.; Sidorko, V.R. Thermodynamic properties of scandium-copper compounds. *Powder Metall. Met. Ceram.* **2006**, *45*, 72–75. [CrossRef]
15. Predel, B. Cu-Sc (Copper-Scandium). In *Zahlenwerte und Funktionen aus Naturwissenschaften und Technik: Macroscopic and Technical Properties of Matter*; Neue, S., Hellwege, K.-H., Landolt, H., Madelung, O., Eds.; Springer: Berlin/Heidelberg, Germany, 1994; pp. 1–2. ISBN 3-540-56073-4.
16. Pöhl, C.; Schatte, J.; Leitner, H. Solid solution hardening of molybdenum–hafnium alloys: Experiments and Modeling. *Mater. Sci. Eng. A* **2013**, *559*, 643–650. [CrossRef]
17. Fleischer, R. Substitutional solution hardening. *Acta Metall.* **1963**, *11*, 203–209. [CrossRef]
18. Labusch, R. A Statistical Theory of Solid Solution Hardening. *Phys. Status Solidi (b)* **1970**, *41*, 659–669. [CrossRef]
19. Gypen, L.A.; Deruyttere, A. The combination of atomic size and elastic modulus misfit interactions in solid solution hardening. *Scr. Metall.* **1981**, *15*, 815–820. [CrossRef]
20. Sherstnev, P. *Physikalisch Basierte Modellierung der Gefügeentwicklung Während des Warmwalzens von Aluminiumlegierungen*; Momentanuniversität Leoben: Leoben, Austria, 2009.
21. Weißbach, W.; Jaroschek, C.; Dahms, M. *Werkstoffkunde Lehrbuch: Strukturen, Eigenschaften, Prüfung*; Springer: Berlin/Heidelberg, Germany, 2015; ISBN 978-3-658-03918-9.
22. Hall, E.O. The Deformation and Ageing of Mild Steel: III Discussion of Results. *Proc. Phys. Soc. B* **1951**, *64*, 747–753. [CrossRef]
23. Petch, N.J. The cleavage strength of polycrystals. *J. Iron Steel Inst.* **1953**, *174*, 25–28.
24. Blum, W.; Li, Y.J.; Chen, J.; Zeng, X.H.; Lu, K. On the Hall–Petch relation between flow stress and grain size. *Int. J. Mater. Res.* **2006**, *97*, 1661–1666. [CrossRef]
25. Hansen, N. Hall–Petch relation and boundary strengthening. *Scr. Mater.* **2004**, *51*, 801–806. [CrossRef]
26. Lugovy, M.; Slyunyayev, V.; Brodnikovskyy, M. Solid solution strengthening in multicomponent fcc and bcc alloys: Analytical approach. *Prog. Nat. Sci. Mater. Int.* **2021**, *31*, 95–104. [CrossRef]
27. Cordero, Z.C.; Knight, B.E.; Schuh, C.A. Six decades of the Hall–Petch effect—A survey of grain-size strengthening studies on pure metals. *Int. Mater. Rev.* **2016**, *61*, 495–512. [CrossRef]
28. Courtney, T.H. *Mechanical Behavior of Materials*, 2nd ed.; Waveland: Long Grove, IL, USA, 2005; ISBN 1577664256.
29. Haasen, P. Verfestigung durch Mischkristallbildung. *Int. J. Mater. Res.* **1964**, *55*, 55–60. [CrossRef]
30. Chen, H. Gefüge und Eigenschaften von Äquiatomaren Legierungen aus dem System Ta-Nb-Mo-Cr-Ti-Al. Ph.D. Thesis, Karlsruher Institut für Technologie (KIT), Karlsruhe, Germany, 2020.
31. Mrotzek, T. Einfluß der Warmumformung auf Die Gefügebildung und Festigkeit der Molybdänlegierung TZM. Ph.D. Thesis, Karlsruher Institut für Technologie (KIT), Karlsruhe, Germany, 2018.
32. Takeuchi, S. On the shear modulus parameter in the theory of solid-solution hardening. *Scr. Metall.* **1968**, *2*, 481–483. [CrossRef]
33. Kratochvíl, P.; Neradová, E. Solid solution hardening in some copper base alloys. *Czech. J. Phys.* **1971**, *21*, 1273–1278. [CrossRef]
34. Ali, N.; Zhang, L.; Liu, D.; Zhou, H.; Sanaullah, K.; Zhang, C.; Chu, J.; Nian, Y.; Cheng, J. Strengthening mechanisms in high entropy alloys: A review. *Mater. Today Commun.* **2022**, *33*, 104686. [CrossRef]
35. Stoller, R.E.; Zinkle, S.J. On the relationship between uniaxial yield strength and resolved shear stress in polycrystalline materials. *J. Nucl. Mater.* **2000**, *283–287*, 349–352. [CrossRef]
36. Wesemann, I.; Hoffmann, A.; Mrotzek, T.; Martin, U. Investigation of solid solution hardening in molybdenum alloys. *Int. J. Refract. Met. Hard Mater.* **2010**, *28*, 709–715. [CrossRef]
37. *ASTM E112-13*; Test Methods for Determining Average Grain Size. ASTM International: West Conshohocken, PA, USA, 2013.
38. Petzow, G. *Metallographisches, Keramographisches, Plastographisches Ätzen*; 7. Aufl. Bd. 1. Materialkundlich-technische Reihe. Gebrüder Borntraeger: Stuttgart, Germany, 2015; ISBN 3443230199.
39. Bach, G. Über der Größenverteilung von Kugelschnitten in durchsichtigen Schnitten endlicher Dicke. *Z Angew Math Mech* **1958**, *38*, 256–258. [CrossRef]
40. Gaul, A. Erzeugung Remanent Stabiler Domänenmuster in Austauschverschobenen Dünnschichtsystemen Mittels Heliumionen-mikroskopie. Ph.D. Thesis, Universität Kassel, Kassel, Germany, 2018.
41. Gorenflo, R. The Tomato Salad Problem In Spherical Stereology R. Gorenflo. In *Ill-Posed and Inverse Problems*; Romanov, V.G., Kabanikhin, S.I., Anikonov, Y.E., Bukhgeim, A.L., Eds.; De Gruyter: Berlin/Heidelberg, Germany, 2002; pp. 127–144. ISBN 9783110942019.
42. *DIN EN ISO 6507-1:2018-07*; Metallische Werkstoffe - Härteprüfung nach Vickers –Teil_1: Prüfverfahren (ISO_6507-1:2018); Deutsche Fassung EN_ISO_6507-1:2018. Beuth Verlag GmbH: Berlin/Heidelberg, Germany, 2018.
43. *DIN EN ISO 7500-1:2018-06*; Metallische Werkstoffe –Kalibrierung und Überprüfung von Statischen Einachsigen Prüfmaschinen–Teil 1: Zug- und Druckprüfmaschinen–Kalibrierung und Überprüfung der Kraftmesseinrichtung (ISO_7500-1:2018); Deutsche Fassung EN ISO 7500-1:2018. Beuth Verlag GmbH: Berlin/Heidelberg, Germany, 2018.
44. *DIN EN ISO 6892-1:2020-06*; Metallische Werkstoffe–Zugversuch–Teil 1: Prüfverfahren bei Raumtemperatur (ISO 6892-1:2019); Deutsche Fassung EN_ISO_6892-1:2019. Beuth Verlag GmbH: Berlin, Germany, 2020.
45. *DIN 50125:2022-08*; Prüfung Metallischer Werkstoffe–Zugproben. Beuth Verlag GmbH: Berlin, Germany, 2022.
46. Simon, N.; Drexler, E.; Reed, R. *Properties of Copper and Copper Alloys at Cryogenic Temperatures. Final Report*; Materials Reliability Div PB-92-172766/XAB; NIST/MONO-177; National Institute of Standards and Technology (MSEL): Boulder, CO, USA, 1992. Available online: <https://www.osti.gov/biblio/5340308> (accessed on 17 May 2024).

47. Zhou, L.; Wang, M.; Peng, K.; Zhu, J.; Fu, Z.; Li, Z. Structure characteristic and its evolution of Cu-W films prepared by dual-target magnetron sputtering deposition. *Trans. Nonferrous Met. Soc. China* **2012**, *22*, 2700–2706. [[CrossRef](#)]
48. Properties–Kupferverband. Available online: <https://kupfer.de/kupferwerkstoffe/kupfer/eigenschaften/?lang=en> (accessed on 20 May 2024).
49. Köster, W.; Speidel, M.O. Der Einfluß der Temperatur und der Korngröße auf die ausgeprägte Streckgrenze von Kupferlegierungen. *Int. J. Mater. Res.* **1965**, *56*, 585–598. [[CrossRef](#)]
50. Smola, B. On the role of solute atom—Dislocation elastic interaction in solid solution hardening of Cu single crystals. *Czech. J. Phys.* **1981**, *31*, 447–452. [[CrossRef](#)]
51. Zhang, J.; Zhang, Y.; Wang, A.; Liang, T.; Mao, Z.; Su, B.; Li, H.; Xie, J. Insight into the Influence of Alloying Elements on the Elastic Properties and Strengthening of Copper: A High-Throughput First-Principles Calculations. *Metals* **2023**, *13*, 875. [[CrossRef](#)]
52. Jax, P.; Kratochvil, P.; Haasen, P. Solid solution hardening of gold and other f.c.c. single crystals. *Acta Metall.* **1970**, *18*, 237–245. [[CrossRef](#)]

Disclaimer/Publisher’s Note: The statements, opinions and data contained in all publications are solely those of the individual author(s) and contributor(s) and not of MDPI and/or the editor(s). MDPI and/or the editor(s) disclaim responsibility for any injury to people or property resulting from any ideas, methods, instructions or products referred to in the content.